

Volumetric Segmentation of Pelvic Organs from MRI Acquisitions

R. Namías¹, M. del Fresno^{2,3}, J. P. D'Amato^{2,4}, M.-E. Bellemare⁵, and M. Vénere^{2,6}

¹ CIFASIS, French Argentine International Center for Information and Systems Sciences, UAM (France) / UNR-CONICET (Rosario - Argentina)

² Instituto PLADEMA, Universidad Nacional del Centro, Tandil - Argentina

³ Comisión de Investigaciones Científicas de la Prov. de Buenos Aires (CIC-PBA), Argentina

⁴ Consejo Nacional de Investigaciones Científicas y Técnicas CONICET, Argentina

⁵ LSIS UMR CNRS 6168 UAM, Marseille - France

⁶ Comisión Nacional de Energía Atómica, Argentina.

namias@cifasis-conicet.gov.ar

marc-emmanuel.bellemare@lsis.org

{mdelfres,jpdamato,venerem}@exa.unicen.edu.ar

Abstract. In this work we present part of a Pelvis Dynamics Modeling System for pre-surgical assistance in the pelvic organ prolapse disease. In this condition, the most common affected organs are the uterus, the bladder and the rectum. The Magnetic Resonance Imaging (MRI) is the gold standard non-invasive imaging technique to evaluate this condition. The MRI's acquisitions provide spatial information that is essential to build tri-dimensional (3D) models and run physical simulations that recreate the prolapse. In these acquisitions, the above mentioned organs, present blurred borders and different textures. Therefore, its extraction is not trivial at all.

We pose an hybrid semi-automatic segmentation strategy which combines Region Growing (RG) and Active Surfaces in MRI scans to retrieve surface meshes of the organs of interest. We show some real cases, one applying the complete process in detail and the others, providing final results attained by the method which shows high quality segmentations achieved with a low computational cost.

Key words: Medical Imaging, Segmentation, Active Surfaces, Magnetic Resonance.

1 Introduction

The pelvic organ prolapse disease is a very common condition in the aged female population [10]. Many women who have had a baby present some degree of pelvic organ prolapse, but it can also occur in women who have never given birth. In most cases, women do not have symptoms at all. However, sometimes surgery must be done to restore the normal structure and function of the female

pelvic organs. Imaging analysis is the most important non-invasive technique that helps in surgery planning.

The project aims at building specific pelvic organ behavior models for each patient, in order to support the surgeon decisions. In the initial steps, dynamic and volumetric MRI are acquired from patients and then the main organs are segmented. Afterwards, geometrical models are extracted from the segmentation results [1]. Therefore, the segmentation step is critical to obtain more accurate geometrical models.

In the last decade, several segmentation techniques were applied to medical imaging studies. Techniques such as thresholding and region growing are commonly used for this purpose. Other advanced approaches, as active contours [5] and level sets are also widely used [11,6,7].

Pimenta et al. [8] propose a 3D model reconstruction of the bladder applying 2D active contour segmentation in each slide of the MR acquisition. This approach not only needs post-processing to create a 3D model from a set of slide contours but also do not take into consideration the extra information provided by space and continuity in 3D which could be greatly useful in the segmentation of soft organs that are not easily distinguishable in the acquisitions. Therefore, our approach uses a hybrid method to directly obtain 3D models using 3D segmentation techniques. The hybrid method employs two different techniques including region growing and active surfaces to segmentate the main female pelvic organs. This approach was previously used in [3] for brain volumetric segmentations.

The paper is organized as follows: in section 2 we describe the segmentation procedure; in section 3 we present some results in different organs and acquisitions; finally, in section 4 conclusions and future work are mentioned.

2 Segmentation Procedure

The input of the process is a DICOM (Digital Imaging and Communication in Medicine: international standard in medical imaging) graylevel 3D MRI. This volume is processed by a tree stage procedure. First, a region growing (RG) technique is applied. Second, the RG output is used to create a triangular 3D surface mesh. This mesh is smoothed and finally sent to the active surface algorithm that finishes the task.

Region Growing Step

The region growing algorithm is quite standard. The expert manually set one or more seeds in the organ of interest. The algorithm keeps a queue with the visited voxels. In the beginning, only the seed indexes are included. For each candidate voxel in the queue we evaluate whether it satisfies the acceptance criterion. If so, all its neighbors, that were not visited before, are placed in the queue and the candidate is added to the region. If not, the voxel is labeled as a border voxel. The algorithm finishes when the candidates queue is empty. In this work,

a 26-neighborhood for each voxel is considered.

The acceptance criterion is the key of the algorithm. As it is described in previous works [12,14], the MRIs not only produce noise images but also have fixed bias in their acquisitions.

Acceptance criterion Two different acceptance criterions were proposed. We define some metrics for them:

- Caracteristic Intensity: $IC(r) = \frac{1}{N(r)} \sum_{v \in S(r)} I(v)$
- Caracteristic Deviation: $\sigma(r) = \sqrt{\frac{1}{N(r)} \sum_{v \in S(r)} [I(v) - IC(r)]^2}$

where $I()$ is the image graylevel intensity, $S(r)$ are the surrounding voxels of the current voxel r and $N(r)$ is the number of neighbors of r .

So we define the first criterion as:

$$s_v^1(k, r) = \frac{|I(v) - IC(r)|}{k\sigma(r)} \leq 1 \quad (1)$$

where, $k > 0$ is a free parameter used to weight the tolerance criterion. Experiments show that values between 1 and 2.5 work well for most cases.

This criterion does not perform well in presence of noise. Noisy voxels are left outside the region when they should be inside. Therefore, in order to avoid this problem a new criterion is used:

$$s_v^2(k, r) = \frac{\sum_{v'} H(1 - s_{v'}^1(k, r))}{N(v)} \geq f \quad (2)$$

where H is a heavyside function applied to each neighbor v' of v and f is a parameter between 0 and 1. H function returns 1 if v' is accepted according to the $s_v^1(k, r)$ criterion, or 0 otherwise. Then, one voxel is accepted only if a fraction of neighbors over the value f are accepted by the first criterion. This last criterion, called the the fraction-neighborhood criterion, is more robust in presence of noise than the first one.

Surface mesh generation

Generally speaking in computer vision, a mesh is a set of points s_i in the space related somehow by a geometric shape. The most common shapes are polygons, triangles, squares (surface meshes) or tetrahedron (volume meshes). In this work, triangular meshes are used.

In order to create a mesh suface of the object of interest, we take the voxels of the border after doing the region growing process. For each voxel in the frontier, we select the face in between the interior and exterior of the ROI. For each face, we draw two triangles in an appropriate way, so their normals point to the

exterior of the ROI. Thus, the vertex are added clockwise to obtain a proper mesh.

The original mesh shape is not very appropriate as input to the active surface technique. Its voxelized shape is not suitable for being evolved by an approximate differential equation towards its final position. Therefore, the whole mesh is smoothed by a geometrical filter described in [13]. The Taubin filter iteratively moves the points of the mesh. The displacement of each vertex depends on the position of its first order edge neighbors. For each point its displacement is calculated by:

$$\Delta s_i = \sum_{s_j \in N(s_i)} \frac{1}{N_i} (s_i - s_j) \quad (3)$$

where $N(s_i)$ are the edge neighbors of s_i and N_i is the number of neighbors. The new position of the vertex s_i in the k^{th} iteration is calculated as:

$$s_i^{k+1} = s_i^k + \{\lambda, \mu\} \Delta s_i^k \quad (4)$$

where $\{\lambda, \mu\}$ are a contractive and a non-contractive parameter of the filter respectively. This is a constant volume low-pass filter. This algorithm is linear in time and space. We only need to know beforehand the neighbors of each point in the mesh.

Active Surface Models

The final stage of the procedure is the active surface model usually called snake. Different techniques were proposed for the evolution of the snake, such as finite differences, finite elements or dynamic programming. A model based on the formulation proposed by McInerney and Terzopoulos [6] is applied, considering that each vertex s_i of the snake mesh evolves according to the following motion equation:

$$\gamma_i = \frac{ds_i}{dt} - a\alpha_i(t) + b\beta_i(t) = q\rho_i(t) + p f_i(t) \quad (5)$$

where $\alpha_i(t)$, $\beta_i(t)$, $\rho_i(t)$ and $f_i(t)$ are the tension, flexion, inflation and external forces respectively, and γ_i is a damping coefficient. The internal energy simulates the characteristics of an elastic membrane. The internal tension and flexion acting on the vertex s_i represent the snake resistance to stretching and bending respectively, and are calculated as:

$$\alpha_i = \frac{1}{m} \sum_{j \in N(i)} s_j(t) - s_i(t) \quad (6)$$

$$\beta_i = \frac{1}{m} \sum_{j \in N(i)} \alpha_j(t) - \alpha_i(t) \quad (7)$$

where $N(i)$ is the set of nodes s_j neighboring the node s_i and m is the number of these neighbors. The respective derivatives correspond to the Laplacian and the squared Laplacian and they are approximated using the umbrella operator by considering the local mesh topology at the node s_i .

The inflation ρ_i and the external force f_i are calculated as:

$$\rho_i(t) = F(I(s_i(t)))n_i(t) \quad (8)$$

where n_i is the unitary vector normal to the surface at node s_i and F is a binary function relating ρ_i to the intensity field I :

$$F(I(s_i(t))) = \begin{cases} +1 & \text{if } \frac{|I(s_i) - CI(r)|}{k\sigma(r)} \leq 1 \\ -1, & \text{otherwise} \end{cases} \quad (9)$$

The local external force which contains the expansion of the snake at significant edges, acts in each node emulating a potential gradient:

$$f_i(t) = G[\varphi(s_i)] \quad (10)$$

where the G is the gradient vector and the potential φ is defined as:

$$\varphi(s_i) = -\text{grad}[FI(s_i)] \quad (11)$$

The scalar gradient is $\text{grad}[\cdot]$ and $FI(s_i)$ is the intensity $I(s_i)$ smoothed with a Gaussian Filter. Since the initial guess provided by the growing process is a close approximation of the final model, Eq. (5) can be solved directly by applying an explicit first-order Euler scheme:

$$s_i^{(t+\Delta t)} = s_i^{(t)} - \frac{\Delta t}{\gamma_i}(-a\alpha^{(t)} + b\beta_i^{(t)} - q\rho_i^{(t)} - pf_i^{(t)}) \quad (12)$$

provided that the time steps are sufficiently small.

The iteration proceeds until the following stop criterion is achieved.

Stop Criterion We use a two parameter stopping criterion. We measure the fraction of points f that moves less than a maximum tolerance distance t_{max} . The parameter t_{max} (tolerance) is maximum displacement tolerance value of a point and f_{min} is the minimal fraction of points that must be under the tolerance t_{max} to achieve the criterion. So, when the fraction of points f that are displaced at most t_{max} is over f_{min} the criterion is achieved.

The advantage of using the RG result to initialize the snake is that the deformation is then limited to minor perturbations requiring fewer iteration steps. The deformable mesh is composed of subvoxel triangular elements, so the final segmentation has subvoxel accuracy and yields a smooth surface representation, matching concavities and convexities that may be present on complex geometries.

3 Results

In this section, we present the segmentation process of the bladder and rectum from different datasets of anonymized patients. We first present the application of the proposed method for one patient (named patient A) and then the meshes extracted from other two cases(B and C).

The whole image processing modules were developed within the context of the Insight ToolKit (ITK)[4]. ITK uses a pipeline architecture so we developed one new processing filter for each segmentation step, taking advantage of all its preexisting input/output tools and data structures suitable for the task.

We employed an Intel(R) Core(TM) i7 CPU 860 @ 2.80 HGz (Quad Core) with Hyper-Threading, RAM memory: 8Gb DDR3 @ 1066 GHz, under the Linux 3.0.0.16 generic kernel(64bits). The total time of each whole segmentation process lasts less than 2 minutes in this equipment.

The results are visualized with **VolView** and **MITK 3M3**, two other open source tools that comprise the Kitware family.

MRI volume image acquisitions were performed with 1.5T PHILIPS *Gyroscan* on the sagital plane. The DICOM image series are input of the segmentation process. The image series resolution is $256 \times 256 \times 110$ and no pre-processing stages were applied to the acquisitions.

Case A

Input In figure 1 we can observe the A patient MRI.

Region Growing Step The region growing process starts by the manual selection of the seeds. Due to image characteristics, we found that more accurate results are obtained using more than one seed (the more seeds we use, the better statistical description of the region we get). If only one seed is used, the segmentation obtained could be uncompleted, hence, we empirically found that at least 3 seeds were necessary in our experiments (rectum and bladder) to obtain good segmentation results. Following, the parameters $f \in [0, 1]$ and k must be explored as to obtain the desired region of interest. Table 1 presents the parameters used in our example.

The output of the RG process is a volume with three different regions. The outside region, the border and the inside region. In figure 2 there is a view of the two segmented organs. The region of interest resulting from this step is represented by a group of voxels.

Surface mesh generation In this stage, the RG output is the input of the ImageToMesh filter. The raw output of the filter is shown in figure 3 (a). Basically,

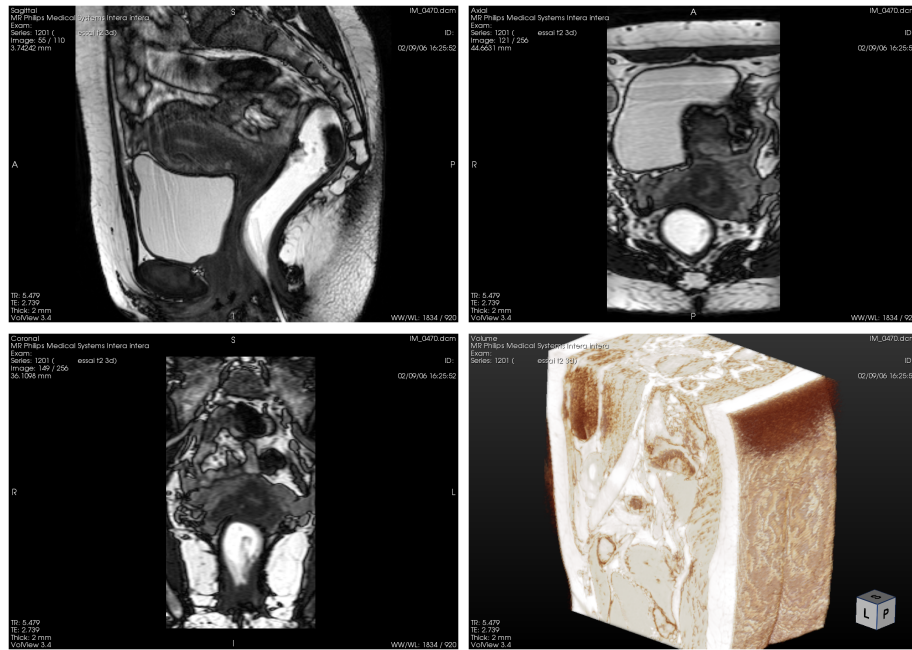


Fig. 1. Patient's A MRI scan: Sagittal View - Axial View | Coronal View - Volume (VolView)

Table 1. Region Growing Parameters

| Bladder | | | | | Rectum | | | | |
|---------|-----|-----|-----|--|--------|-----|-----|-----|--|
| Seeds | x | y | z | | Seeds | x | y | z | |
| I | 101 | 166 | 18 | | I | 155 | 176 | 57 | |
| II | 63 | 132 | 75 | | II | 190 | 117 | 77 | |
| III | 55 | 130 | 43 | | III | 190 | 130 | 50 | |
| k: | 2.3 | f: | 0.5 | | k: | 1.7 | f: | 0.5 | |

the mesh is voxelized, with discontinuous steps which are inconvenient for being evolved as a snake. After applying the Taubin filter (figure 3 (b)) the mesh is smoother than the original (figure 3 (a)).

Active Surface Models In the final stage, the snake takes the smooth mesh and runs until the stop criterion is achieved, one for each organ. Several parameters must be tuned to obtain a good segmentation result. These are the flexion force a , the tension force b , the inflation force q and the extern force p . Also, the integrations step Δt , and the stop criterion ones: tolerance t and fraction f . All these parameters must be adjusted according the type of organ under analysis. For example an organ like brain or rectum will need a more flexible surface snake than bladder or lung. That is why in the bladder segmentation the a

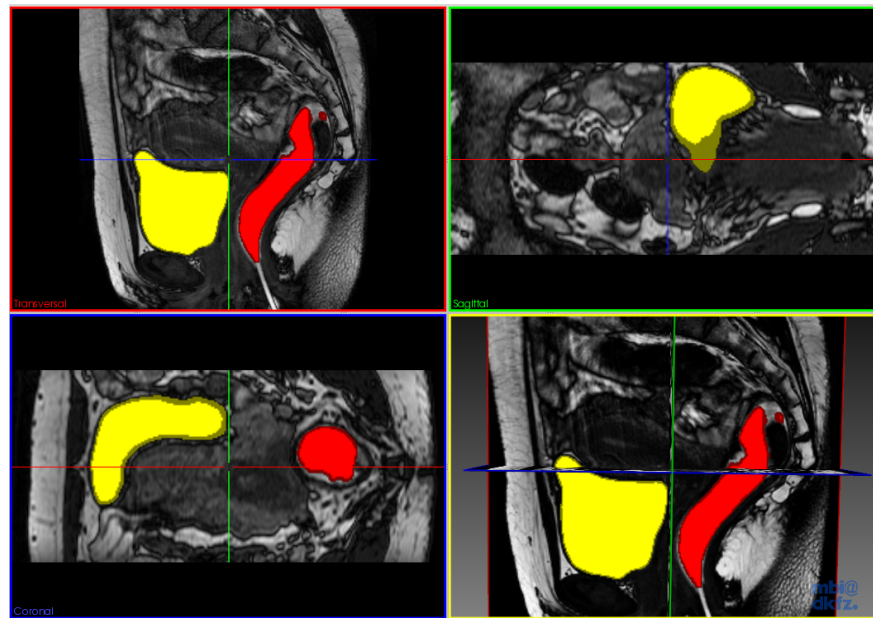


Fig. 2. View of the RG output over the original scan. Bladder(yellow), Rectum(red). The darker pixels are the border pixels

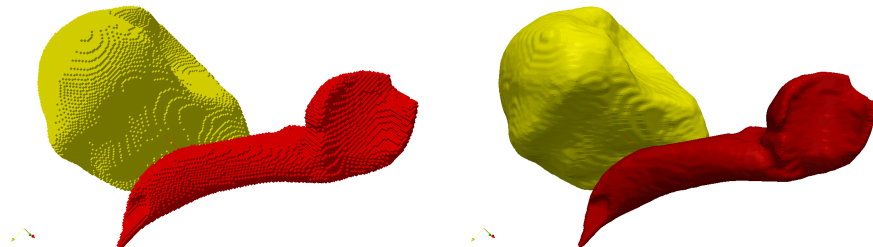


Fig. 3. Meshes: Bladder(yellow) and Rectum(red) - (a) Original Mesh - (b) Smoothed Mesh

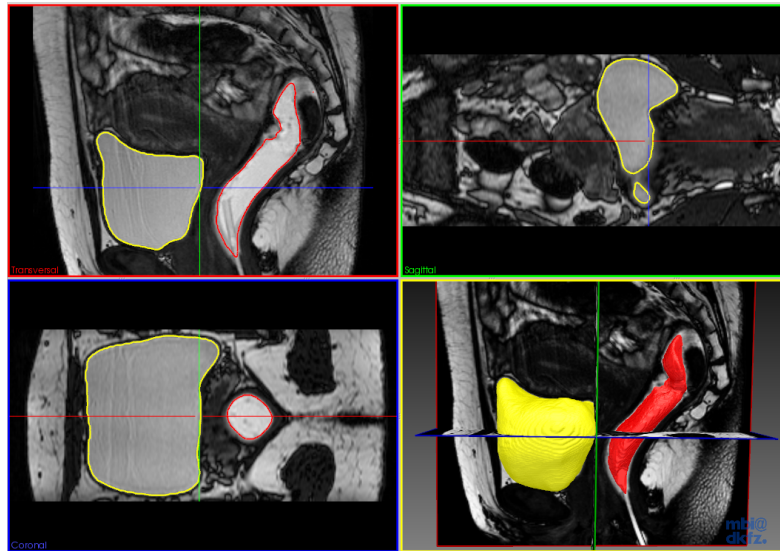
and b parameters are higher than for the rectum case to obtain a softer mesh representation. Table 2 presents the parameters used in our example.

Cases B and C

We present segmentations results for other two patients, called B and C. Figures 5 and figure 6 are the final results of the segmentation process. Several methods exist [15,9,2] to evaluate the segmentation quality. Nevertheless, in these cases the gold standard is not available so results were evaluated by visual inspection. Segmentations were considered by the experts as reasonable good.

Table 2. Snake Parameters

| Bladder | | Rectum | |
|-------------------|--------|-------------------|--------|
| a: 6.0 | b: 5.6 | a: 4.2 | b: 3.5 |
| p: 1.0 | q: 2.3 | p: 1.2 | q: 2.4 |
| f: 0.8 | t: 0.2 | f: 0.7 | t: 0.3 |
| Δt : 0.01 | | Δt : 0.01 | |

**Fig. 4.** View of the snake output over the original scan. Bladder(yellow), Rectum(red).

4 Conclusions

We have presented a hybrid method for segmenting pelvic organs in volumetric MRI acquisitions. These acquisitions are quite noisy and the structures of interest are not easily distinguishable. Our technique gives good results for segmenting two of the desired organs, bladder and rectum. Nevertheless, it does not work appropriately for the uterus since this organ is not easy distinguishable from its context.

The final segmentation meshes have a smooth shape and a sub-voxel precision, two desired properties. Although no gold standards are available, the quality of the segmentation was evaluated visually by an expert giving good results.

The main contribution of this work is to build an automatic segmentation system that assist in surgery procedures. The obtained results show us that the

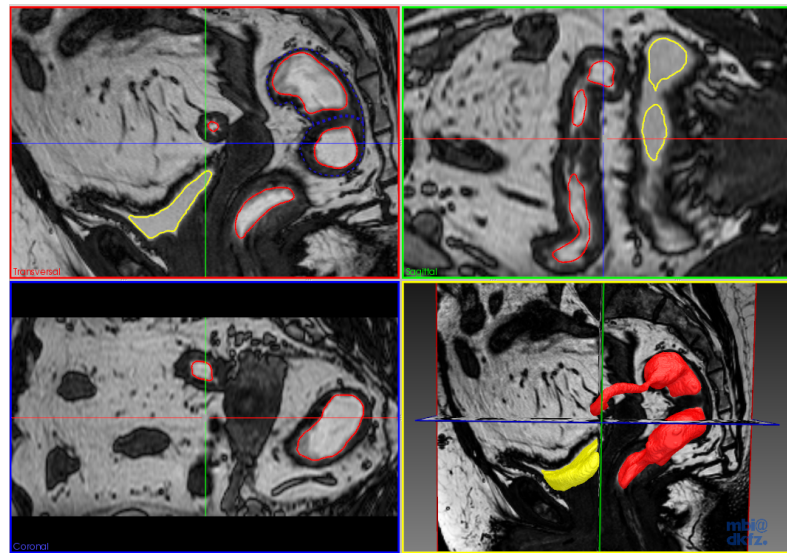


Fig. 5. Patient B - Snake output over the original scan. Bladder(yellow), Rectum(red)

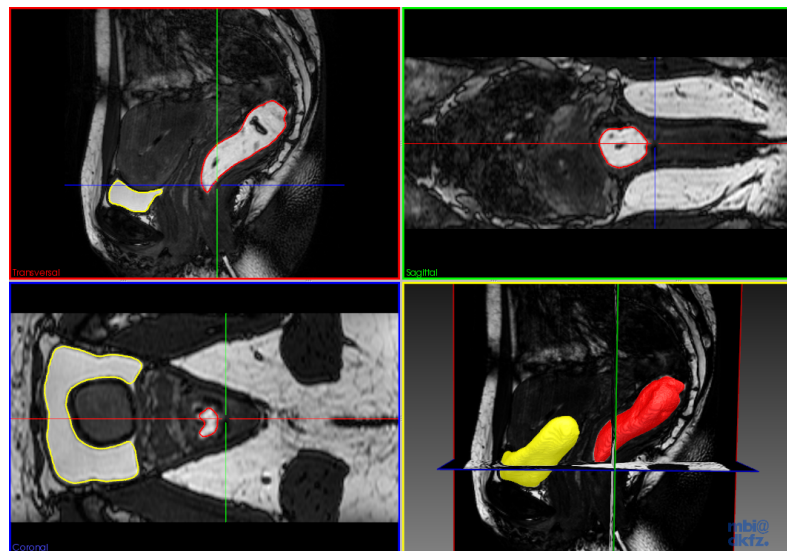


Fig. 6. Patient C - Snake output over the original scan. Bladder(yellow), Rectum(red)

proposed strategy is effective. However, more complex cases such as the uterus needs the development of new techniques. e

Future Work

Different problems occur during the segmentation process. The most important one is the difficulty to achieve the uterus segmentation. The uterus region is neither homogeneous nor contrasting within its neighborhood. The RG technique here described, fails to obtain a good starting mesh for the snake stage. Other image features descriptors, such as texture, must be used.

Moreover, the mesh evolution presents its own problems. In some cases, the mesh produces self-collisions when two or more triangles overlap during movement. These collisions must be prevented because in these cases the resulting surface mesh will have topological errors. So, a self-colliding detector could be implemented to solve this problem.

In the rectum segmentation, only the detection of its internal part is done. The rectal walls are not negligible as the bladder's, therefore, we are sub-segmentating the organ. In figure 5, in the transversal view we can appreciate the contour in blue of the rectal wall outside the red perimeter of the snake. This part must be reconsidered in order to have a more accurate physical model. We propose a 2-step snake stage for segmenting not homogeneous organs such as the rectum. Finally, regarding the segmentation quality, although it is very hard to manually segmentate a 3D volume slice by slice, we planned anyway to obtain manual segmentations of the organs provided by experts in imaging diagnosis to use as a *gold standard* and quantify the accuracy of the segmentation process. Also we plan to work with images from different patients and analyze if the strategy is robust enough and the parameters used can be fixed.

References

1. T. Bay, J.-C. Chambelland, R. Raffin, M. Daniel, and M.-E. Bellemare. Geometric modeling of pelvic organs. In *Engineering in Medicine and Biology Society,EMBC, 2011 Annual International Conference of the IEEE*, pages 4329 –4332, 30 2011-sept. 3 2011.
2. V. Chalana and Y. Kim. A methodology for evaluation of boundary detection algorithms on medical images. *IEEE Trans. Med. Imaging*, 16(5):642–652, 1997.
3. M. del Fresno, M. Vénere, and A. Clausse. A combined region growing and deformable model method for extraction of closed surfaces in 3d ct and mri scans. *Computerized Medical Imaging and Graphics*, 33(5):369 – 376, 2009.
4. L. Ibanez, W. Schroeder, L. Ng, and J. Cates. *The ITK Software Guide*. Kitware, Inc. ISBN 1-930934-15-7, <http://www.itk.org/ItkSoftwareGuide.pdf>, second edition, 2005.
5. M. Kass, A. Witkin, and D. Terzopoulos. Snakes: Active contour models. *INTERNATIONAL JOURNAL OF COMPUTER VISION*, 1(4):321–331, 1988.
6. T. Mcinerney and D. Terzopoulos. Topology adaptive deformable surfaces for medical image volume segmentation. *IEEE Transactions on Medical Imaging*, 18:840–850, 1999.
7. S. Osher and R. P. Fedkiw. Level set methods. In *in Imaging, Vision and Graphics*. Springer, 2000.

8. S. Pimenta, J.M. Tavares, R.N. Jorge, F. Alexandre, T. Mascarenhas, and R. El Sayed. Reconstruction of 3d models from medical images: Application to female pelvic organs, October 2006.
9. A. Popovic, M. de la Fuente, M. Engelhardt, and K. Radermacher. Statistical validation metric for accuracy assessment in medical image segmentation. *International Journal of Computer Assisted Radiology and Surgery*, 2:169–181, 2007. 10.1007/s11548-007-0125-1.
10. Boreham M. Schaffer J., Wai C. Etiology of pelvic organ prolapse. *Clin Obstet Gynecol*, 48:639–47, 2005.
11. A. Singh, D. Terzopoulos, and D.B. Goldgof. *Deformable Models in Medical Image Analysis*. IEEE Computer Society Press, Los Alamitos, CA, USA, 1st edition, 1998.
12. M. Styner, C. Brechbuhler, G. Szekely, and G. Gerig. Parametric estimate of intensity inhomogeneities applied to mri. *Medical Imaging, IEEE Transactions on*, 19(3):153 –165, march 2000.
13. G. Taubin. A Signal Processing Approach to Fair Surface Design. *Computer Graphics*, 29(Annual Conference Series):351–358, 1995.
14. U. Vovk, F. Pernus, and B. Likar. A review of methods for correction of intensity inhomogeneity in mri. *Medical Imaging, IEEE Transactions on*, 26(3):405 –421, march 2007.
15. S. Warfield, K. Zou, and W. Wells. Validation of image segmentation and expert quality with an expectation-maximization algorithm. In Takeyoshi Dohi and Ron Kikinis, editors, *Medical Image Computing and Computer-Assisted Intervention - MICCAI 2002*, volume 2488 of *Lecture Notes in Computer Science*, pages 298–306. Springer Berlin / Heidelberg, 2002.